Quadruped leg design principles for handling slopes or high-speed running

Ioannis Kontolatis[*], Ioannis Poulakakis[#] and Evangelos Papadopoulos[*]

[*] School of Mechanical Engineering
National Technical University of Athens
9 Heroon Polytechniou Str.,
15780 Athens, Greece
[ikontol, egpapado]@central.ntua.gr

[#] Department of Mechanical Engineering
University of Delaware
130 Academy Street, Newark,
DE 19716-3140, U.S.A.
poulakas@udel.edu

ABSTRACT

Research work in legged locomotion has resulted in leg concept designs that address a number of technical issues. Although these works concluded with proof of concept results, they have not offered specific guidelines regarding leg design options or comparisons between alternative leg designs. In this paper, multibody analysis and simulations using the Matlab and MSC Adams software were conducted to define guidelines related to two fundamental aspects in leg design. *Design Aspect 1*: which is the optimum knee joint orientation for a quadruped robot that traverses straight-ahead (a) a sloped terrain and (b) a level terrain at maximum speed? *Design Aspect 2*: which is the optimum degree of freedom (DOF), actuated DOF and compliance elements position for a quadruped that traverses straight-ahead (i) a sloped terrain and (ii) a level terrain at maximum speed? Results show that the answer to the first question is that the frontwards knee joint orientation reduces torque demands for knee joint, especially for the rear knee joint. Regarding the second question, results show that for a quadruped robot that traverses straight-ahead on a sloped terrain, leg architecture should exploit an actuated knee joint to increase mechanism workspace, robot capability for ground clearance and adequate traction. Compliance should be located at the lowest part of the leg. For a quadruped robot that traverses straight-ahead on a level terrain at maximum speed, the optimum leg architecture is characterized by the minimum suspended mass and by highest frequency oscillations.

Keywords: Quadruped robots, leg design, multibody systems.

1 INTRODUCTION

Humans and animals have incredible motion capabilities in terms of speed, energy efficiency and capacity for transversing environments with extreme slopes. These capabilities are due mainly to their legged locomotion system that allows them to use discrete footprints in handling terrain discontinuities. Also, they modify muscle stiffness and centre of mass (CoM) location to preserve their desired motion in an efficient way, despite ground inclinations. In addition, humans and animals are able to perform dynamically stable motions, so as to achieve high speeds.

Engineers have already acknowledged the potential advantages of legged locomotion, and presented leg concept designs that address technical issues. In [1], the robot FastRunner utilizes a leg architecture, which incorporates a network of elastic elements and uses a single main drive actuator as a power source. Ananthanarayanan et al. applied to leg design the hypothesis that employing a tendon-bone co-location architecture not only provides leg compliance, but can also reduce bone stresses caused by bending [2]. Hutter et al. introduced and compared two compliant robotic legs that perform precise joint torque and position control, enabling passive adaptation to the environment, and allowing for the exploitation of natural dynamics motions [3]. Semini et al. designed an articulated/-segmented leg, suitable for a versatile robot that runs, hops and navigates over rough terrain [4]. Kontolatis and Papadopoulos have shown that an optimum region of leg spring constant and uncompressed length emerges for level and sloped (positive/ negative) terrain traversal [5].

Although these research works have concluded with proof of concept results, they did not offer specific guidelines about leg design options. To the best of our knowledge, no comparison between alternative leg designs has been performed so far. Taking the above into consideration, in our current work we perform multibody analysis and conduct simulations using the Matlab and MSC Adams software to define guidelines for two fundamental aspects of leg design. Our results show that a frontward knee joint orientation reduces torque demands, especially for the rear knee joint. We also show that for a quadruped robot that traverses straight-ahead a sloped terrain, an actuated knee is useful in increasing mechanism workspace, robot capability for ground clearance, and adequate traction, while compliance should be located at the lowest part of the leg. For a quadruped robot that traverses straight-ahead a level terrain at maximum speed, minimum suspended mass and highest frequency oscillations are desired.

2 DESIGN ASPECT 1 - KNEE JOINT ORIENTATION

The question addressed here is: which is the optimum knee joint orientation for a quadruped robot that traverses straight-ahead (a) a sloped terrain and (b) a level terrain at maximum speed? Fig. 1 displays some possible answers to this question.

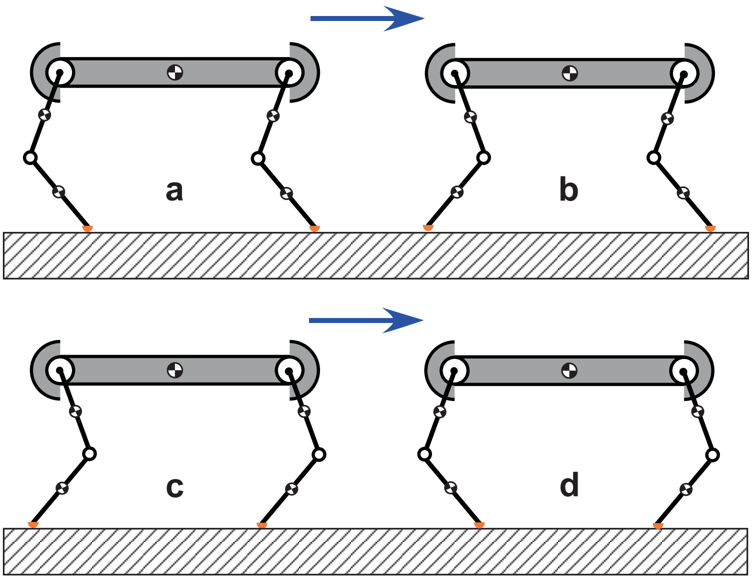

Figure 1. Knee joint orientation design options. (a) Both backwards, (b) Rear frontwards-Front backwards, (c) Both frontwards and (d) Rear backwards-Front frontwards.

2.1 Force-Torque Analysis

The legs in a multibody robot system can be seen as mechanisms transmitting forces and torques to the main body. However, for this to happen, the actuators must be able to deliver the required for some motion torques. However, even if actuators can apply unlimited torques, the requirements may not be met due to other reasons, such as limits placed by friction developed at leg endpoints. Therefore, it is important to analyse leg mechanisms from the standpoint of force-torque transmission.

Force - torque equilibrium analysis and free-body diagrams are used to calculate hip and knee torque quantities. The robot model presented in Fig. 2, is planar and consists of two massless *virtual legs* and a body of mass m. A virtual leg, front or rear, models the two respective physical legs that operate in pairs when a gait is realized. A virtual leg exerts torques and forces on the body equal to those by the two physical ones [6]. The model is studied when both virtual legs touch the ground, forming a closed chain mechanism with the ground, and while they apply torques to move the body forward with acceleration α. Forces and torques applied to the robot links, and length and angle quantities of the links and joints respectively are presented also in Fig. 2 for the case of knee joint orientation shown in Fig. 1 (b). By altering the values of angles γ_1 and γ_2, cases (a), (c) and (d) can be studied too.

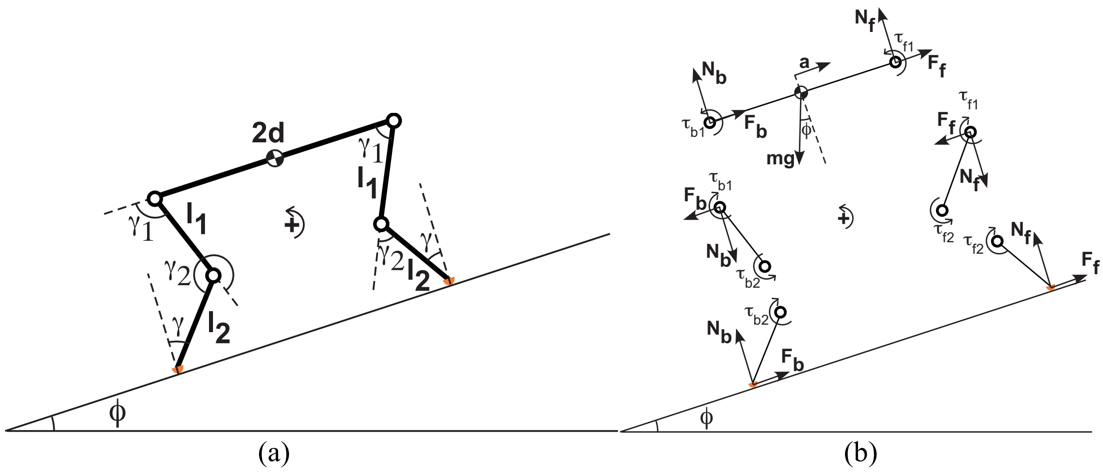

Figure 2. (a) Definition of robot parameters, (b) free body diagram with forces and torques.

Using force and torque equilibrium equations for each link, the following equations are derived:

Back Lower Leg (torque equilibrium)

$$N_b \cdot l_2 \cdot \sin(\gamma) + F_b \cdot l_2 \cdot \cos(\gamma) - \tau_{b2} = 0 \tag{1}$$

Back Upper Leg (torque equilibrium)

$$N_b \cdot l_1 \cdot \cos(\pi - \gamma_1) + F_b \cdot l_1 \cdot \sin(\pi - \gamma_1) - \tau_{b1} + \tau_{b2} = 0 \tag{2}$$

Front Lower Leg (torque equilibrium)

$$N_f \cdot l_2 \cdot \sin(\gamma) + F_f \cdot l_2 \cdot \cos(\gamma) - \tau_{f2} = 0 \tag{3}$$

Front Upper Leg (torque equilibrium)

$$N_f \cdot l_1 \cdot \cos(\pi - \gamma_1) + F_f \cdot l_1 \cdot \sin(\pi - \gamma_1) - \tau_{f1} + \tau_{f2} = 0 \tag{4}$$

Main Body (two force equilibrium, one torque equilibrium equations)

$$F_b + F_f - m \cdot g \cdot \sin(\varphi) = m \cdot a \tag{5}$$

$$N_b + N_f - m \cdot g \cdot \cos(\varphi) = 0 \tag{6}$$

$$-N_b \cdot d + N_f \cdot d + \tau_{b1} + \tau_{f1} = 0 \tag{7}$$

The equation that connects touchdown angle γ and joint angles γ_1 and γ_2 is:

$$\gamma = (\gamma_1 + \gamma_2) - (\pi / 2) \tag{8}$$

Let τ_{b1} and a be the independent variables (inputs) in Eqs. (1)-(7). Then, these written as:

$$\mathbf{A} \cdot \mathbf{x} = \mathbf{b} \tag{9}$$

where

$$A = \begin{bmatrix} l_2 \sin(\gamma) & l_2 \cos(\gamma) & 0 & 0 & -1 & 0 & 0 \\ -l_1 \cos(\gamma_1) & l_1 \sin(\gamma_1) & 0 & 0 & 1 & 0 & 0 \\ 0 & 0 & l_2 \sin(\gamma) & l_2 \cos(\gamma) & 0 & 0 & -1 \\ 0 & 0 & -l_1 \cos(\gamma_1) & l_1 \sin(\gamma_1) & 0 & -1 & 1 \\ 0 & 1 & 0 & 1 & 0 & 0 & 0 \\ 1 & 0 & 1 & 0 & 0 & 0 & 0 \\ -d & 0 & d & 0 & 0 & 1 & 0 \end{bmatrix} \tag{10}$$

$$x = \begin{bmatrix} N_b \\ F_b \\ N_f \\ F_f \\ \tau_{b2} \\ \tau_{f1} \\ \tau_{f2} \end{bmatrix} \qquad and \qquad b = \begin{bmatrix} 0 \\ \tau_{b1} \\ 0 \\ 0 \\ ma + mg\sin(\varphi) \\ mg\cos(\varphi) \\ -\tau_{b1} \end{bmatrix} \tag{11}$$

The matrix **A** is invertible; the system solution **x** is presented in the Appendix.

For stability during quadruped robot forward acceleration, the front leg ground reaction force should be greater or equal to zero (marginal value), i.e. $N_f \geq 0$. Solving Eq. (10) for N_f:

$$N_f = \frac{-(\mathrm{m}(\alpha l_2\cos(\gamma) - \mathrm{dg}\cos(\varphi) - \mathrm{g}l_1\cos(\gamma_1+\varphi) + \alpha l_1\sin(\gamma_1) + \mathrm{g}l_2\sin(\gamma + \varphi))}{2\mathrm{d}} \tag{12}$$

and substituting in $N_f \geq 0$, an inequality for the half hip-to-hip distance d results:

$$d \geq \frac{l_1(\alpha\cdot\mathrm{n}\cdot\cos(\gamma) + \mathrm{g}\cdot\cos(\gamma_1\text{-}\varphi)+\alpha\cdot\sin(\gamma_1)\text{-}\mathrm{g}\cdot\mathrm{n}\cdot\sin(\gamma\text{-}\varphi))}{\mathrm{g}\cos(\varphi)} \tag{13}$$

where

$$n = l_2 / l_1 \tag{14}$$

In addition, ground reactions must lie inside the leg friction cone, i.e.:

$$\left|\frac{F_f}{N_f}\right| < \mu, \qquad \left|\frac{F_b}{N_b}\right| < \mu \tag{15}$$

Using the solution of Eq. (10) for F_f, N_f, F_b and N_b in Eq. (15), the bounds for the rear hip torques $\tau_{b1,\min}$ and $\tau_{b1,\max}$ are calculated so that the front and rear leg stay in contact with the ground. Two more bounds are identified using the solution of Eq. (10) for the front leg torque τ_{f1} and ground friction F_f. The τ_{f1} should be equal or greater than zero so that the front hip torque is not antagonizing the back one, increasing energy consumption. Also, the F_f must be non-negative, so that the front leg does not to slip forward.

2.2 Results

The analysis presented in Section 2.1 defines areas for valid hip and knee joint torques during forward quadruped motion. The results are presented in the following plots.

Fig. 3 displays the admissible range of back hip joint torques as a function of foot-ground friction coefficient in the static case (α = 0) and the quasi-static case, with (α = 2 m/s). The parameters used are shown in the figure. We note that the admissible region of torques is quite small; therefore the system controller must be designed very carefully if it is desired to avoid slippage, tipping, or excessive power usage.

Fig. 4 displays the admissible range of hip joint torques as a function of the ground inclination for φ values between 0 to 25 degrees. As expected, the required torques increase with the inclination rapidly. Therefore, for given torque bounds of the actuation system, this plot allows computation of the maximum slope the robot can negotiate.

In Fig. 5 bounds for admissible hip joint torques as a function of the robot acceleration are given. The analysis is conducted for α values 0 to 3 m/s^2. Again, higher accelerations require higher torques, with narrow range between the min and max bounds for some α.

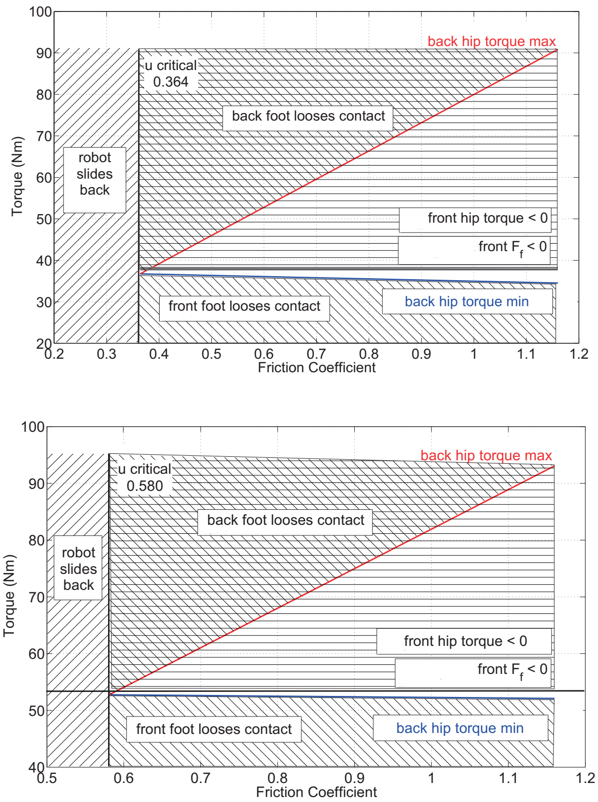

(a)

(b)

Figure 3. Back hip joint torque bounds vs. the foot-ground friction coefficient for (a) static (α = 0 m/s^2) and (b) quasi-static case (α = 2 m/s^2). m= 30 kg, d= 0.3 m, γ_1= 130 deg, γ_2= 280 deg, l_1=l_2=0.15 m.

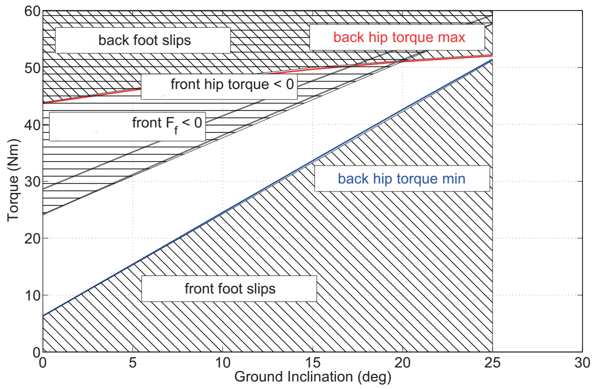

Figure 4. Back hip joint torque bounds vs. the ground inclination. m = 30 kg, α = 2.0 m/s^2, μ = 0.7, d = 0.3 m, γ_1 = 130 deg, γ_2 = 280 deg, l_1 = l_2 = 0.15 m.

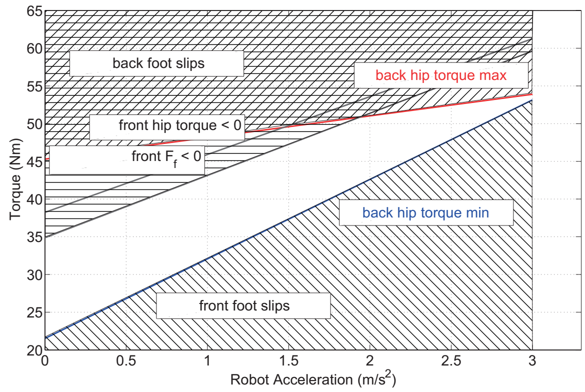

Figure 5. Back hip joint torque limits vs. the robot acceleration. m = 30 kg, μ = 0.7, d = 0.3 m, γ_1 = 130 deg, γ_2 = 280 deg, l_1 = l_2 = 0.15 m.

Fig. 6 displays the boundaries of admissible hip joint torques as a function of the half hip-to-hip distance. The analysis is conducted for d between 0.2 to 0.5 m. In Fig. 7, the bounds of admissible hip joint torques as a function of the leg link ratio n are presented. The analysis is conducted for n values between 0.5 to 1.5.

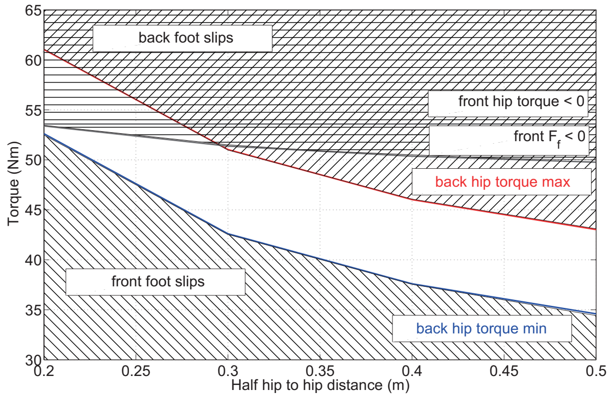

Figure 6. Back hip joint torque limits vs. the half hip-to-hip distance. m = 30 kg, α = 2.0 m/s^2, μ = 0.7, γ_1 = 130 deg, γ_2 = 280 deg, $l_1 = l_2$ = 0.15 m.

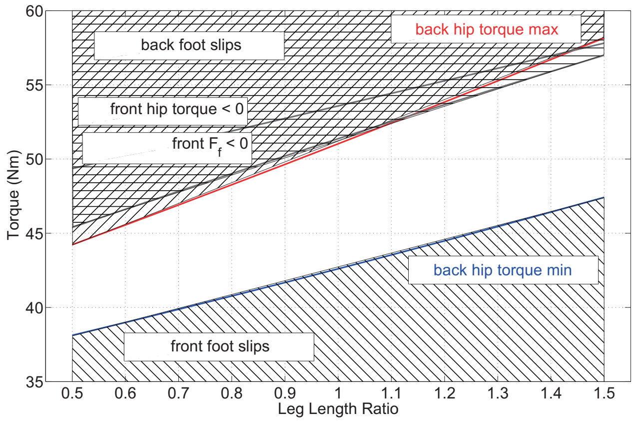

Figure 7. Back hip joint torque limits vs. the leg links length ratio. m = 30 kg, α = 2.0 m/s^2, μ = 0.7, d = 0.3 m, γ_1 = 130 deg, γ_2 = 280 deg.

A comparison between the magnitude of hip and knee joint torques as a function of the robot acceleration is presented in Fig. 8. Therefore, the critical actuators are the hip ones.

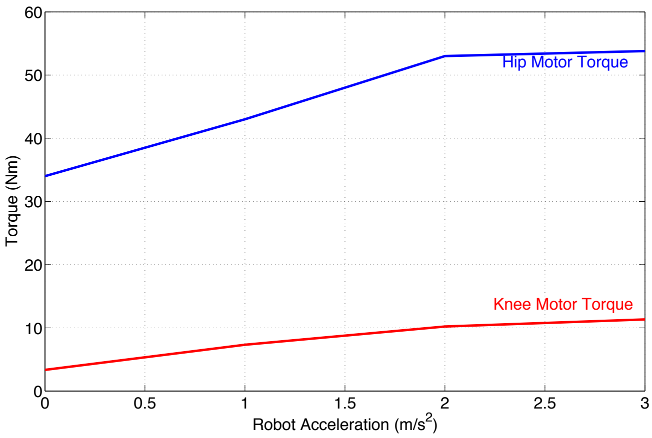

Figure 8. Back hip and knee joint torque magnitude vs. the robot acceleration. m = 30 kg, μ = 0.7, d = 0.3 m, γ_1 = 130 deg, γ_2 = 280 deg.

We can now proceed to discussing which is the optimum knee joint orientation for a quadruped that traverses straight-ahead in (a) a sloped terrain and (b) a level terrain at maximum speed.

The results for case (a) are presented in Table 1 for a quadruped that moves forward at a terrain of inclination φ = 20 deg using different knee joint orientation. It should be noted here that the analysis is conducted for the back leg because this leg contributes the most when the robot ascends. As can be seen in Table 1, when a quadruped robot traverses straight-ahead a sloped terrain, the frontward knee joint orientation reduces torque demands for the knee joint, especially for the rear knee joint τ_{b2}, i.e. 4.71 vs. 22.71 Nm.

Table 1. Rear and front, hip and knee joint torque absolute values (Nm) for forward acceleration α = 1 m/s^2 and terrain inclination φ = 20 deg.

Leg Orientation	τ_{b1} (Nm)	τ_{b2} (Nm)	τ_{f1} (Nm)	τ_{f2} (Nm)
Frontward orientation	18.00	4.71	2.02	3.05
Backward orientation	18.00	22.71	2.02	5.07

The results for level terrain at maximum speed are presented in Table 2 for a quadruped that moves forward with acceleration α = 3 m/s^2 using alternative knee joint orientation. Table 2 shows that when a quadruped robot traverses straight-ahead a level terrain at maximum speed, again the frontward knee joint orientation reduces torque demands for knee joint, especially for the rear knee joint torques τ_{b2}, i.e. 8.51 vs. 26.51 Nm.

Table 2. Rear and front, hip and knee joint torque absolute values (Nm) for forward acceleration α = 3 m/s^2 and terrain inclination φ = 0 deg.

Leg Orientation	τ_{b1} (Nm)	τ_{b2} (Nm)	τ_{f1} (Nm)	τ_{f2} (Nm)
Frontward orientation	18.00	8.51	2.68	9.52
Backward orientation	18.00	26.51	2.68	12.21

3 DESIGN ASPECT 2 - LEG MECHANISM CHARACTERISTICS

The question to be addressed here is what is the optimum DOF, actuated DOF and compliance elements location for a quadruped that traverses straight-ahead (a) a sloped terrain and (b) a level terrain with the maximum speed. Fig. 9 displays some of the alternative architectures that can be considered. These two leg design questions are answered taking into consideration the following design goals for both sloped terrain and high-speed level terrain motion:

- low suspended mass,
- low energy consumption,
- low mechanical complexity,
- adequate traction to achieve maximum motor torque usage,
- durability to impact and torsional loads.

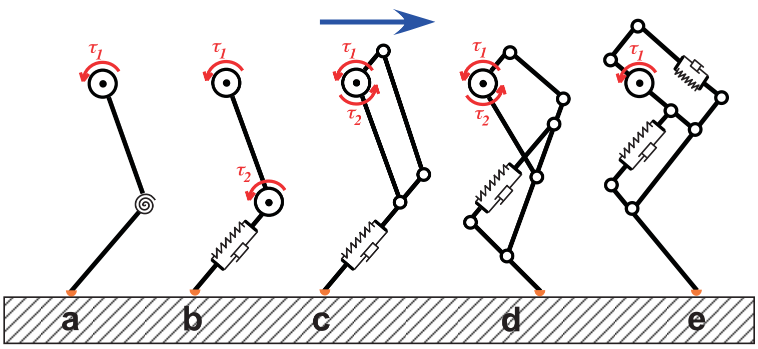

Figure 9. Leg architectures. (a) Single actuator (hip), torsion spring (knee), (b) Two actuators (hip, knee), linear spring (ankle), (c) Two actuators (hip), 4-bar link, linear spring (ankle), (d) Two actuators (hip), two 4-bar links, linear spring (ankle) and e) One actuator (hip), two 4-bar links, linear spring (ankle).

For effective leg design, two more points are taken into consideration; for high-speed running, all legs should oscillate at high frequencies and be able to perform large angle trajectories in the sagittal plane, while for sloped terrain motion, the legs should be able to move in both the sagittal and coronal planes.

With reference to Fig. 9, although option (a) meets the first two specifications, the passive knee joint limits leg workspace and the capability for ground clearance and adequate traction. The same holds for option (e) in which the suspended mass is higher than (a) due to the network of linear and nonlinear elastic elements. In addition, the elastic elements network adds mechanical complexity. Both options i.e. (a) and (e) can be optimized for specific motion characteristics and if these change, the leg mechanism parameters need to be calculated again. Due to this last reason, options (a) and (e) are eliminated for sloped terrain handling.

Leg architecture option (b) is the worst regarding the first specification, i.e. the low suspended mass, because knee joint actuator is mounted at a distant joint. For this reason, it is should be not considered for high-speed running. Also, it results in higher energy consumption than that for options (a) and (e), but increased knee joint workspace, ground clearance capability and adequate traction due to the actuated knee joint.

Although leg architecture options (c) and (d) have higher energy consumption than options (a) and (e) due to the actuated knee joint, they all have the advantage of option (b) without the disadvantage of high suspended mass because the knee joint actuator is mounted on the robot body. The increased mechanical complexity is surpassed by the suspended mass reduction.

In conclusion, for a quadruped robot that traverses straight-ahead in a sloped terrain, leg architecture option (c) is the most appropriate solution because it exploits an actuated knee joint that increases mechanism workspace and robot capability for ground clearance, and adequate traction. Also, compliance is located at the lowest part of the leg, therefore it receives an impact force directly and provides space at the upper part of the leg for the third hip joint actuator that moves leg in coronal plane. For a quadruped robot that traverses straight-ahead on a level terrain with maximum speed, leg architecture option (d) is the most appropriate solution because it has the lowest suspended mass and can achieve high frequency oscillations.

4 SIMULATIONS

To validate the results presented above, simulations were conducted using the multibody dynamics software MSC Adams. The quadruped robot model, presented in Fig. 10, has massless legs with 2 links, 0.14 m each. The body weighs 20 kg and provides hip-to-hip distance 0.4 m and 0.2 m at the sagittal and coronal plane respectively.

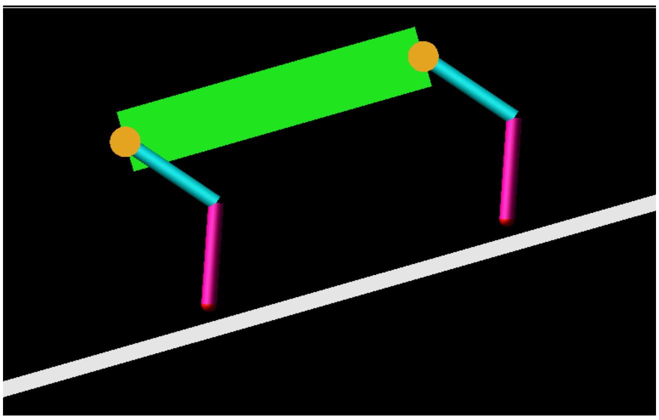

Figure 10. MSC Adams quadruped robot model.

Using the 3D robot model, simulations were conducted for the four knee joint orientation cases (Fig. 1) and the results are presented in Fig. 11. With reference to this figure, in cases (a) and (b) only a hip and a knee torque plot are presented because the other are identical to those. As one can observe, in all cases hip joint torques are high and equal, but knee joint torques differ. The results are consistent with the theoretical analysis performed in Section 2.1 and the case (c) i.e. both knees have frontward orientation, has the lowest values for knee joint torques. Case (a) is the worst, as both knee joints demand the highest torque values, while cases (b) and (d) need high torque on one knee and low torque on the other.

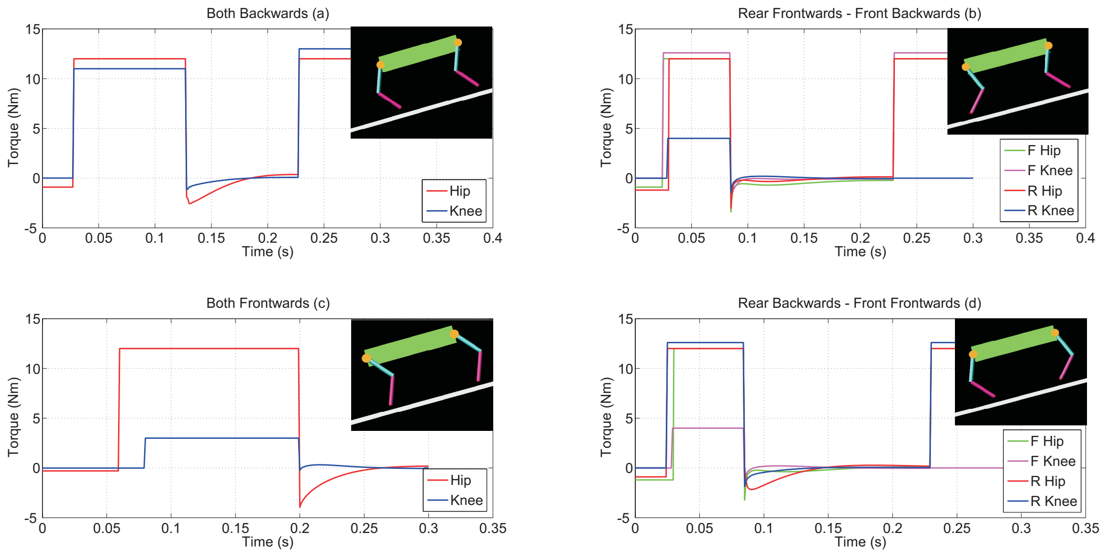

Figure 11. 3D model joint torque results for (a) Both backwards, (b) Rear frontwards-Front backwards, (c) Both frontwards and (d) Rear backwards-Front frontwards.

5 CONCLUSIONS

In this work, two fundamental aspects of leg design were defined as most important for leg locomotion performance and answered using specific criteria. *Design Aspect 1*: which is the optimum knee joint orientation for a quadruped robot that traverses straight-ahead (a) a sloped terrain and (b) a level terrain at maximum speed? *Design Aspect 2*: which is the optimum DOF, actuated DOF and compliance elements position for a quadruped that traverses straight-ahead on a sloped terrain and on a level terrain with maximum speed?

Results show that the answer for the first question is that the frontwards knee joint orientation reduces torque demands for knee joint, especially for the rear knee joint. For the second question, results show that for a quadruped robot that traverses straight-ahead on a sloped terrain, leg architecture should exploit an actuated knee joint to increase mechanism workspace, robot capability for ground clearance and adequate traction. Compliance should be located at the lowest part of the leg. For a quadruped robot that traverses straight-ahead on a level terrain with the maximum speed, leg architecture should have the lowest suspended mass and achieve high frequency oscillations.

ACKNOWLEDGMENT

This research has been financed by the European Union (European Social Fund – ESF) and Greek national funds through the Operational Program “Education and Lifelong Learning” of the National Strategic Reference Framework (NSRF) – Research Funding Program: ARISTEIA: Reinforcement of the interdisciplinary and/ or inter-institutional research and innovation.

In addition, the authors would like to thank Mr Athanasios Mastrogeorgiou for providing the 3D model in MSC Adams software and his valuable help.

REFERENCES

[1] S. Cotton, I. M. C. Olaru, M. Bellman, T. van der Ven, J. Godowksi, and J. Pratt. Fastrunner: A fast, efficient and robust bipedal robot. Concept and planar simulation. *In Proc. 2012 IEEE International Conference on Robotics and Automation (ICRA),* pp. 2358-2364, St. Paul, Minnesota, USA, May, 2012.

[2] A. Ananthanarayanan, M. Azadi, and S. Kim. Towards a bio-inspired leg design for high-speed running. *Bioinspiration & Biomimetics*, Vol. 7, No. 4, 046005, 2012.

[3] M. Hutter, C. D. Remy, M. A. Hoepflinger, and R. Siegwart. Efficient and versatile locomotion with highly compliant legs. *IEEE/ ASME Transactions on Mechatronics*, Vol. 18, No. 2, pp. 449-458, 2013.

[4] C. Semini, N. G. Tsagarakis, E. Guglielmino, M. Focchi, F. Cannella, and D. G. Caldwell. Design of HyQ – a hydraulically and electrically actuated quadruped robot. *In Proc. of the Institution of Mechanical Engineers, Part I: Journal of Systems and Control Engineering*, 0959651811402275, 2011.

[5] I. Kontolatis and E. Papadopoulos. Gravity and inclination effects on the design of quadruped robots for space exploration. *In Proc. of the 21st Mediterranean Conference on Control & Automation (MED)*, pp. 1362-1367, Chania, Crete, Greece, 2013.

[6] M. Raibert. *Legged Robots That Balance*, MIT Press, Cambridge, MA, 1986, pp. 92-95.

APPENDIX

The system solution **x** of Eq. (10) is:

$$N_b = \frac{\mathrm{m}(\alpha l_2\mathrm{c}(\gamma)+\mathrm{g}l_1\mathrm{c}(\gamma_1\text{-}\varphi)+\mathrm{dgc}(\varphi)+\alpha l_1\mathrm{s}(\gamma_1\text{- }\mathrm{g}l_2\mathrm{s}(\gamma\text{-}\varphi))}{2\mathrm{d}} \tag{16}$$

$$\begin{aligned} F_b &= (4\mathrm{d}\tau_{b1}\text{-}2\mathrm{m}(l_1\mathrm{c}(\gamma_1)\text{-}l_2\mathrm{s}(\gamma)) \\ &\frac{(\alpha l_2\mathrm{c}(\gamma)+\mathrm{g}l_1\mathrm{c}(\gamma_1\text{-}\varphi)+\mathrm{dgc}(\varphi)+\alpha l_1\mathrm{s}(\gamma_1)\text{-}\mathrm{g}l_2\mathrm{s}(\gamma\text{-}\varphi)))}{4\mathrm{d}(l_2\mathrm{c}(\gamma)+l_1\mathrm{s}(\gamma_1))} \end{aligned} \tag{17}$$

$$N_f = \frac{\text{-}(\mathrm{m}(\alpha l_2\cos(\gamma)\ \text{-}\ \mathrm{dg}\cos(\varphi)\ \text{-}\ \mathrm{g}l_1\cos(\gamma_1+\varphi)\ +\ \alpha l_1\sin(\gamma_1)+\mathrm{g}l_2\sin(\gamma\ +\ \varphi))}{2\mathrm{d}} \tag{18}$$

$$\begin{aligned} F_f &= \frac{\text{-}2\mathrm{d}\tau_{b1}+\mathrm{m}(\mathrm{gc}(\varphi)(l_1\mathrm{c}(\gamma_1)\text{-}l_2\mathrm{s}(\gamma))(\mathrm{d}+l_1\mathrm{c}(\gamma_1)\text{-}l_2\mathrm{s}(\gamma))}{2\mathrm{d}(l_2\mathrm{c}(\gamma)+l_1\mathrm{s}(\gamma_1))}+ \\ &\frac{\alpha(2\mathrm{d}+l_1\mathrm{c}(\gamma_1)\text{-}l_2\mathrm{s}(\gamma))(l_2\mathrm{c}(\gamma)+l_1\mathrm{s}(\gamma_1))+\mathrm{g}(2\mathrm{d}+l_1\mathrm{c}(\gamma_1)\text{-}l_2\mathrm{s}(\gamma))(l_2\mathrm{c}(\gamma)+l_1\mathrm{s}(\gamma_1))\mathrm{s}(\varphi))}{2\mathrm{d}(l_2\mathrm{c}(\gamma)+l_1\mathrm{s}(\gamma_1))} \end{aligned} \tag{19}$$

$$\begin{aligned} \tau_{b2} &= \frac{\text{-}2\mathrm{d}\tau_{b1}+\mathrm{m}(\mathrm{gc}(\varphi)(l_1\mathrm{c}(\gamma_1)\text{-}l_2\mathrm{s}(\gamma))(\mathrm{d}+l_1\mathrm{c}(\gamma_1)\text{-}l_2\mathrm{s}(\gamma))}{2\mathrm{d}(l_2\mathrm{c}(\gamma)+l_1\mathrm{s}(\gamma_1))}+ \\ &\frac{\alpha(2\mathrm{d}+l_1\mathrm{c}(\gamma_1)\text{-}l_2\mathrm{s}(\gamma))(l_2\mathrm{c}(\gamma)+l_1\mathrm{s}(\gamma_1))+\mathrm{g}(2\mathrm{d}+l_1\mathrm{c}(\gamma_1)\text{-}l_2\mathrm{s}(\gamma))(l_2\mathrm{c}(\gamma)+l_1\mathrm{s}(\gamma_1))\mathrm{s}(\varphi))}{2\mathrm{d}(l_2\mathrm{c}(\gamma)+l_1\mathrm{s}(\gamma_1))} \end{aligned} \tag{20}$$

$$\tau_{f1} = \text{-}\tau_{b1}+\alpha l_2\mathrm{mc}(\gamma)+\mathrm{g}l_1\mathrm{mc}(\gamma_1-\varphi)+\alpha l_1\mathrm{ms}(\gamma_1)\text{-}\mathrm{g}l_2\mathrm{ms}(\gamma\text{-}\varphi) \tag{21}$$

$$\begin{aligned} \tau_{f2} &= \frac{l_2(4dl_2mc(\gamma)^2(a+gs(\varphi))+c(\gamma)(-4d\tau_{b1}+gmc(\varphi)(l_1^2-4dl_2s(\gamma))}{4\mathrm{d}(l_2\mathrm{c}(\gamma)+l_1\mathrm{s}(\gamma_1))} \\ &\frac{+2l_1l_2mc(\gamma-\gamma_1)(a+gs(\varphi))+4dl_1ms(\gamma_1)(a+gs(\varphi)))+l_1m(gl_1c(\gamma-2\gamma_1)c(\varphi)+2(dgc(\gamma+\gamma_1)c(\varphi)}{4\mathrm{d}(l_2\mathrm{c}(\gamma)+l_1\mathrm{s}(\gamma_1))} \\ &\frac{+c(\gamma-\gamma_1)(-gl_2c(\varphi)s(\gamma)+l_1s(\gamma_1)(a+gs(\varphi))))))}{4\mathrm{d}(\mathrm{l}_2\mathrm{c}(\gamma)+\mathrm{l}_1\mathrm{s}(\gamma_1))} \end{aligned} \tag{22}$$